PROCEEDINGS OF SCIENCE

# Lepton flavour universality tests using $B^0 \to D^{*-}\tau^+\nu_\tau$ with muonic and hadronic $\tau$ decays

**Guy Wormser***

*On behalf of the LHCb collaboration,*
*IJCLab,*
*Paris-Saclay University and IN2P3/CNRS, Orsay, France*

*E-mail:* guy.wormser@ijclab.in2p3.fr

Three complementary tests of Lepton Flavour Universality (LFU) using semitauonic $B$ decays performed by the LHCb collaboration are reported : the first LHCb combined measurement of $R(D^{*-})$ and $R(D^0)$ using muonic $\tau$ decay channel, the update of the $R(D^{*-})$ measurement based on hadronic $\tau$ decay channel and the first LHCb measurement of the $D^{*-}$ polarization in this decay channel. The two latter measurements are the most precise single measurements to date. In particular, using 2 fb$^{-1}$ of proton-proton collision data at a centre-of-mass energy of 13 TeV, the ratio $\mathcal{B}(B^0 \to D^{*-}\tau^+\nu_\tau)/\mathcal{B}(B^0 \to D^{*-}\pi^+\pi^-\pi^+)$ is found be $1.70 \pm 0.10^{+0.11}_{-0.10}$, where the first uncertainty is statistical and the second systematic. The lepton universality test, $\mathcal{R}(D^{*-}) \equiv \mathcal{B}(B^0 \to D^{*-}\tau^+\nu_\tau)/\mathcal{B}(B^0 \to D^{*-}\mu^+\nu_\mu)$ is found to be $0.257 \pm 0.012\,(\text{stat}) \pm 0.014\,(\text{syst}) \pm 0.012\,(\text{ext})$, after inclusion of the previously published Run1 result. This result is compatible with SM prediction and with previous measurements. Using these recent LHCb results, the updated word average $R(D^*)$ and $R(D)$ however still displays a 3.3 $\sigma$ disagreement with the SM prediction.

The $D^{*-}$ polarization, which is a powerful complementary test of a potential LFU violation, has been measured for the first by the LHCb collaboration using the same hadronic semitauonic $B^0$ decays in two $q^2$ bins and been found to be: $0.51 \pm 0.07\,(\text{stat}) \pm 0.03\,(\text{syst}), 0.35 \pm 0.08\,(\text{stat}) \pm 0.02\,(\text{syst})$ and $0.43 \pm 0.06\,(\text{stat}) \pm 0.03\,(\text{syst})$, for $q^2$ below 7 GeV$^2/c^4$, above 7 GeV$^2/c^4$ and integrated over all $q^2$ values, respectively. This result, the most precise to date, is compatible with SM predictions and could potentially exclude some phase space regions of New Physics models where the polarization is very different from SM expectations.

*21st Conference on Flavor Physics and CP Violation (FPCP 2023)*
*29 May - 2 June 2023*
*Lyon, France*

*Speaker





PoS(FPCP2023)052

## 1. Introduction

The ratio of branching fraction $\mathcal{R}(D^{(*)}) \equiv \mathcal{B}(B^0 \to D^{(*)}\tau^+\nu_\tau)/\mathcal{B}(B^0 \to D^{(*)}\ell^+\nu_\ell)$, with $\ell = \mu, e$, is predicted by the Standard Model (SM) to a per-cent level accuracy and can therefore be used as a stringent test of lepton flavour universality (LFU) in $b \to c\ell\nu_\ell$ charged-current transitions. This ratio has been measured over the last ten years by the Babar [1], Belle [2, 3] and LHCb [4–6] collaborations using different $\tau$ decay channels and diverse selection methods. A detailed review of these measurements can be found in [7]. A persistent discrepancy between the world-average values of $\mathcal{R}(D^*)$ and $\mathcal{R}(D)$ measurements with their theoretical prediction is at the level of 3.3 standard deviations [8], including the very recent Belle-II preliminary measurement [9]. Several new physics (NP) extensions to the SM can explain this anomaly, *e.g.* leptoquark models [10–12], which typically assume a leptoquark that preferentially couples to third-generation leptons and has a mass below 1 TeV/$c^2$. Three recent results from the LHCb experiment are presented in this paper: a combined $\mathcal{R}(D^*)$-$\mathcal{R}(D)$ measurement using the $\tau$ muonic decay , an update of the $\mathcal{R}(D^*)$ measurement based on the 3-prong $\tau$ decay channel and a precise measurement of the $D^{*-}$ polarization in $B^0 \to D^{*-}\tau^+\nu_\tau$ decays. This measurement represents an further powerful independent LFU test since various NP models can lead to rather different $D^{*-}$ polarization values even if the corresponding $\mathcal{R}(D^*)$ yield does not deviate from the SM prediction [13, 14].

## 2. Detector and simulation

The LHCb detector [15, 16] is a single-arm forward spectrometer covering the pseudorapidity range $2 < \eta < 5$, designed for the study of particles containing $b$ or $c$ quarks. The detector includes a high-precision tracking system consisting of a silicon-strip vertex detector surrounding the $pp$ interaction region [17], a large-area silicon-strip detector located upstream of a dipole magnet with a bending power of about 4 Tm, and three stations of silicon-strip detectors and straw drift tubes [18, 19] placed downstream of the magnet. The tracking system provides a measurement of the momentum, $p$, of charged particles with a relative uncertainty that varies from 0.5% at low momentum to 1.0% at 200 GeV/$c$. The minimum distance of a track to a primary $pp$ collision vertex (PV), the impact parameter (IP), is measured with a resolution of $(15 + 29/p_{\rm T})$ μm, where $p_{\rm T}$ is the component of the momentum transverse to the beam, in GeV/$c$. Different types of charged hadrons are distinguished using information from two ring-imaging Cherenkov (RICH) detectors [20]. Photons, electrons and hadrons are identified by a calorimeter system consisting of scintillating-pad and preshower detectors, an electromagnetic and a hadronic calorimeter. Muons are identified by a system composed of alternating layers of iron and multiwire proportional chambers [21].

The online event selection is performed by a trigger [22], which consists of a hardware stage, based on information from the calorimeter and muon systems, followed by a software stage, which applies a full event reconstruction. At the hardware-trigger stage, events are required to have a muon with high $p_{\rm T}$ or a hadron, photon or electron with high transverse energy in the calorimeters. The hadron can originate from either the decay chain under consideration or the remainder of the event. The software trigger requires a two-, three- or four-track secondary vertex with a significant displacement from any PV. At least one charged particle must have a transverse

momentum $p_T > 1.6\,\text{GeV}/c$ and be inconsistent with originating from any PV. A multivariate algorithm [23, 24] is used for the identification of secondary vertices consistent with the decay of a $b$ hadron.

Large samples of simulated events are required to reduce the systematic uncertainty due to the sample size. A fast simulation technique, ReDecay [25], is used for this purpose in which the underlying $pp$ interaction is reused multiple times, with an independently generated signal decay for each. These samples have been validated against simulated events using unique underlying interactions.

## 3. The combined $\mathcal{R}(D^*)$-$\mathcal{R}(D)$ measurement using the $\tau^+ \to \mu^+\nu_\mu\overline{\nu}_\tau$ channel

Using the muonic $\tau$ decay channel, the LHCb collaboration recently performed a combined measurement of $\mathcal{R}(D^*)$-$\mathcal{R}(D)$, based of 3 $\text{fb}^{-1}$ of collider data taken at $\sqrt{s}$ of 7 and 8 TeV [26]. Fig 1 summarizes the main results. The missing mass to the $D^{(*)-}\mu$ system and the muon energy in the reconstructed $B$ rest-frame distributions are shown at high $q^2$ for both $\overline{D}^0\mu^+$ and $D^{*-}\mu^+$ final states. In addition to a very tight muon identification, an essential selection requirement is that no other charged particle is compatible with the $B$ or $D$ vertices beyond those forming the $D^{(*)}\mu$ system Thanks to the very high statistics available, a clear signal component is visible above a significant background originating from double-charm events where the second charm meson, mostly a $D^+$ meson, underwent a semileptonic decay. This illustrates the critical need to monitor as accurately as possible this background source. This is achieved in particular by using a distinct control sample where an extra-kaon is reconstructed together with $D$ and the muon, a final state characteristic of this background. A good agreement is observed in this control sample with the simulation, enabling the precise measurement of the semitauonic decays. The other major source of systematic uncertainty for this measurement, [26], is the feed-down due to the semimuonic decay of the $B$ hadron to an highly excited $D$ state, either a resonant $D^{**}$ state, or a non resonant $D\pi$ or $D\pi\pi$ state. This is also constrained by a dedicated $D\pi\mu$ control sample, but a better knowledge of these decays will be highly beneficial. In the long run, the limitation due to the finite size of the simulation samples will need to be reduced by advanced computing techniques.

## 4. Update of the $\mathcal{R}(D^*)$ measurement with three-prong hadronic $\tau$ decay using 13 TeV data

The LHCb collaboration pioneered in 2017 the use of the three-prong $\tau$ decay to measure $B$ semitauonic events [5, 6]. This decay channel has several key advantages:

- it allows to measure the $\tau$ decay vertex with an excellent precision, allowing a three-orders-of magnitude suppression of the so called "prompt" background $B^0 \to D^{*-}\pi^+\pi^-\pi^+$ X where the three pions originate from the $B$ decay point,

- the final state contains only two neutrinos, which allows to reconstruct, using the $B$ and $\tau$ approximate lines of flights, the full event kinematics with a precision as good as 15%

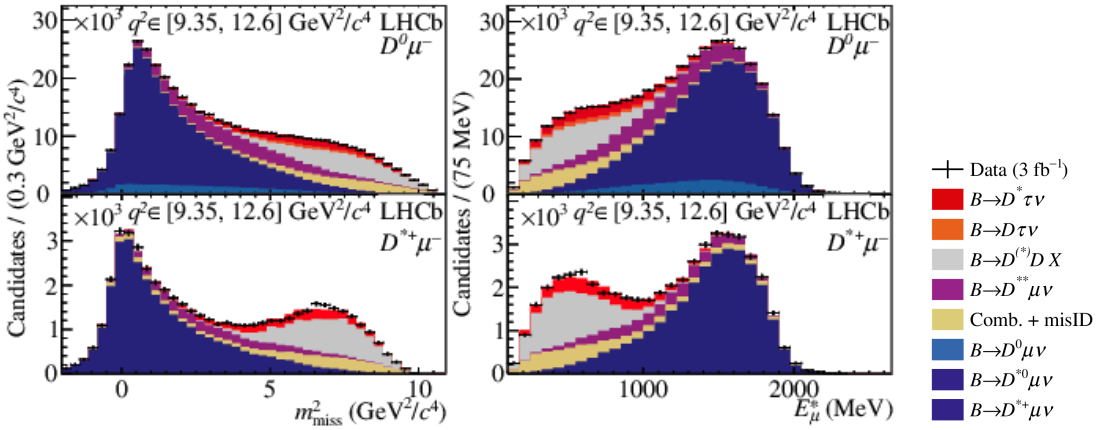


**Figure 1:** Distributions of (left) the missing mass m2miss and (right) in the highest $q^2$ bin (above 9.35 GeV$^2/c^4$) of the (top) $D^0\mu^-$ and (bottom) $D^{*+}\mu^-$ signal data, overlaid with projections of the fit model.

- the strong difference between the dynamics of the three-pion system in $\tau$ decays and in $D_s^+$ decays, the dominant background after suppression of the prompt background mentioned above, allows to isolate the signal candidates with a good purity

- there is no equivalent to the problematic $D^{**}\mu$ feed-down background since its analogous $D^{**}3\pi$ channels are part of the prompt background and highly suppressed.

The results presented here are extracted from the recent update of the $\mathcal{R}(D^*)$ measurement by the LHCb collaboration with 2 fb$^{-1}$ of 13 TeV proton-proton collisions[27]. At this center of mass energy, the $b\bar{b}$ cross section is twice larger than for Run1 data. In addition, several improvements were introduced in LHCb, both at the trigger and analysis level.

### 4.1 Event selection

Signal candidates are formed by combining a $D^{*-}$ meson that decays as $D^{*-} \to \pi^- \overline{D}^0 (\to K^+\pi^-)$ and a $3\pi$ system forming a good vertex. To reject the main background, called hereafter prompt background, where the $3\pi$ system comes promptly from the $B^0$ vertex, the distance between the $B^0$ and $3\pi$ vertices along the beam direction, $\Delta z \equiv z(3\pi) - z(B^0)$, is required to be about four times its uncertainty ($\sigma_{\Delta z}$). Double-charm $B \to D^{*-}D(X)$ decays are the next dominant background, with a detached vertex topology similar to that of the signal decays. Tracks consistent with a kaon or pion hypothesis and having $p > 2\,\text{GeV}/c$ and $p_\text{T} > 250\,\text{MeV}/c$ are selected to form $\overline{D}^0$ candidates, which are required to have a mass in the range [1840, 1890] MeV/$c^2$ and $p_\text{T}$ larger than 1.2 GeV/$c$. The $\overline{D}^0$ candidates are then combined with tracks consistent with the pion hypothesis and with $p_\text{T} > 110\,\text{MeV}/c$ to form $D^{*-}$ candidates, where the difference in the masses of the $D^{*-}$ and $\overline{D}^0$ candidates ($\Delta m$) must lie within 143 and 148 MeV/$c^2$. Sideband regions of $m(\overline{D}^0)$ in ranges [1825, 1840] MeV/$c^2$ and [1890, 1905] MeV/$c^2$ and $\Delta m$ within [150, 160] MeV/$c^2$ are defined to study the combinatorial background. The $\tau^+$ candidates are formed from three tracks, where each track must have $p_\text{T} > 250\,\text{MeV}/c$ and be consistent with the pion hypothesis.

The charged pion and kaon tracks must be positively identified using the information provided by the particle identification (PID) system [6]. Contamination due to decays of the type $B \to D^{*-}D^+(X)$, with the subsequent decay $D^+ \to K^-\pi^+\pi^+(\pi^0)$, are suppressed by requiring that the kaon identification probability is less than 17% for the $\pi^-$ candidate within the $3\pi$ system.

The combinatorial background is further suppressed using a boosted decision tree (BDT) classifier that is trained using simulated $B^0 \to D^{*-}\tau^+\nu_\tau$ decays as the signal proxy and the data sample with the same-sign charge combination $D^{*-}\pi^-\pi^+\pi^-$ as the background proxy. This BDT classifier rejects about 75% of the combinatorial background while preserving 77% of the $B^0 \to D^{*-}\tau^+\nu_\tau$ decays.

A closely related challenge is the rejection of background candidates with more than six charged tracks. The main source of these candidates are $B \to D^{*-}D_s^+(X)$ processes where the $D_s^+$ meson decays into five stable charged particles and $B \to D^{*-}D^0K^+$ decays where the $D^0$ meson decays into four stable charged particles. A dedicated algorithm [28] is used to evaluate the isolation of each signal-candidate track from other non-signal tracks in an event. An isolation BDT classifier is formed from this information for each signal-candidate track, trained using simulated $B^0 \to D^{*-}\tau^+\nu_\tau$ decays as the signal proxy and simulated $B \to D^{*-}D^0K^+$ decays in which two extraneous charged kaons are present as the background proxy. This classifier removes 82% of background decays with extra charged tracks while retaining 78% of signal decays. The signal-mode $B^0 \to D^{*-}\tau^+\nu_\tau$ candidates are identified with the use of a detached-vertex criterion and a targeted suppression of backgrounds where $D_s^+$ decays mimic hadronic decays of $\tau^+$ leptons. In $B^0 \to D^{*-}\tau^+\nu_\tau$ decays, the $3\pi$ vertex is detached from the $B^0$ vertex. A good approximation for the $B^0$ vertex is the point of closest approach between the $D^{*-}$ line of flight and the $3\pi$ line of flight. A BDT classifier is used to identify this detached topology. The inputs to this BDT classifier are the positions of the $\overline{D}^0$, $B^0$ and $3\pi$ vertices and their related uncertainties, the $3\pi$ mass, and the momenta of the tracks forming the $B^0$ candidate. The training of this BDT is performed using simulated $B^0 \to D^{*-}\tau^+\nu_\tau$ decays as signal and simulated prompt $b\overline{b} \to D^{*-}3\pi X$ production as background samples. The efficiency and rejection performance of this BDT classifier is slightly better than the beam-direction significance used in Refs. [5, 6]; the rejection rate is 20% higher for the same signal efficiency.

The $3\pi$ decay of the $\tau^+$ proceeds predominantly through an $a_1$ resonance with a $\rho^0\pi^+$ intermediate state. The major background contribution due to $D_s^+$ decays to $3\pi(X)$ primarily proceeds through $\eta$ and $\eta'$ resonances, with only a very small contribution from $Ra_1$ structures, where $R$ designates an $\eta, \eta', \omega, \phi$ or $K^0$ meson [29]. The $\pi^+\pi^-$ mass is kinematically limited to $< 400\,\mathrm{MeV}/c^2$ for the decays $\eta \to \pi^+\pi^-\pi^0$ and $\eta' \to \pi^+\pi^-\eta$, which provides input to a discriminating variable formed by the minimum mass of the two $\pi^+\pi^-$ combinations present in the pion triplet. The $3\pi$ system from $D_s^+$ decays is often accompanied with a large number of neutral particles from the same decay. Variables related to the energy from these neutral particles in cones around the $3\pi$ system direction are used in a BDT classifier to suppress these backgrounds. This classifier is trained using simulated $B^0 \to D^{*-}\tau^+\nu_\tau$ events as the signal training sample and simulated $D_s^+$ events decaying into three pions as the background training sample. The performance of this anti-$D_s^+$ BDT is better than that found in the previous analysis [5, 6] with 40% rejection of $D_s^+$ events for a 97% signal efficiency. The anti-$D_s^+$ BDT output is used as a fit variable to estimate the yield of $B^0 \to D^{*-}\tau^+\nu_\tau$ decays. An upper boundary for the invariant mass of the of the $3\pi$ system and of $D^*3\pi$ candidates

is set at 1600 and 5100 MeV/$c^2$,respectively, consistent with the presence of neutrinos in the final state of the signal decays. After all the selection requirements are applied, only 0.5% of events have multiple candidates, from which one is chosen at random.

The selection efficiencies ($\varepsilon$) for $B^0 \to D^{*-}\tau^+\nu_\tau$ and $B^0 \to D^{*-}3\pi$ modes are estimated from simulation after corrections are applied. The respective efficiencies are $\varepsilon_{\rm sig} = (1.05 \pm 0.01) \times 10^{-4}$ and $\varepsilon_{\rm norm} = (3.00 \pm 0.03) \times 10^{-4}$. The uncertainties are due to the limited size of the simulation samples.

### 4.2 Study of double-charm background

The dominant background category after applying the selection criteria is double-charm decays $B \to D^{*-}D(X)$, where $D$ is a $D_s^+$, $D^+$ or $D^0$ meson. Given the importance of the $D_s^+$ background, it is necessary to model the inclusive $D_s^+$ decays to $3\pi$ as well as possible. Note that, although the exclusive decay $D_s^+ \to \pi^+\pi^-\pi^+$ has a small branching fraction, 1%, the inclusive decays $D_s^+ \to \pi^+\pi^-\pi^+$ X have a branching fraction as large as 32%, as recently measured by the BES-III collaboration [30]. The decomposition of this inclusive rate in the 50 different channels contributing to this final state is not very well known. Therefore, the fractions of different $D_s^+ \to 3\pi X$ decays are determined from a data sample enriched in these decays, with a reverse requirement on the anti-$D_s^+$ BDT output. A simultaneous binned maximum-likelihood fit is performed to the distribution of four variables: $\min[m(\pi^+\pi^-)]$, $\max[m(\pi^+\pi^-)]$, $m(\pi^+\pi^+)$, and $m(3\pi)$. The different $D_s^+$ decay components are broadly divided into four categories:

- $D_s^+ \to \eta\pi^+(\pi^0)$ decays where charged pions from the $\eta$ meson are selected;
- $D_s^+ \to \eta'\pi^+(\pi^0)$ decays where charged pions from the $\eta'$ meson are selected;
- $D_s^+ \to \omega\pi^+(\pi^0)$ or $D_s^+ \to \phi\pi^+(\pi^0)$ decays where charged pions from the $\omega$ or $\phi$ meson are selected;
- $D_s^+$ decays where the pions originate either directly from the $D_s^+$ decay or from the $a_1$ resonance: $\eta 3\pi$, $\eta a_1$, $\eta' 3\pi$, $\eta' a_1$, $\omega 3\pi$, $\omega a_1$, $\phi 3\pi$, $\phi a_1$, $K^0 3\pi$, $K^0 a_1$, $\tau^+\nu_\tau$ and non-resonant $3\pi$.

The template PDFs for the various $D_s^+$ decay components are defined using inclusive $B \to D^{*-}D_s^+X$ simulation samples, and the non-$D_s^+$ decays are modelled using the inclusive $B \to D^{*-}3\pi X$ simulation sample. The fraction of each of the four $D_s^+$ decay components, relative fractions of $\eta 3\pi$, $\eta' 3\pi$ and $\omega 3\pi$ final states and the total number of $D_s^+$ and non-$D_s^+$ decays are free parameters in the fit. Compared to the previous analysis [5, 6], the simulated samples are improved with the addition of $D_s^+ \to Ra_1$ modes with $R \in \{\eta, \eta', \omega, \phi, K^0\}$, which enable a more detailed description of the $D_s^+ \to 3\pi X$ decay. This introduces more fit parameters and hence additional constraints are applied to ensure the stability of the fit. The fit assumes no interference effects, as a full amplitude analysis is beyond the scope of this study. The fit results are given in Fig. 2, which shows the fractions of the four inclusive categories mentioned above. The relative fraction $D_s^+ \to Ra_1/(D_s^+ \to Ra_1 + D_s^+ \to R3\pi)$ is fixed at 5.5%. The fractions of $D_s^+$ decays to $\phi a_1 + \phi 3\pi$, $K^0 a_1 + K^0 3\pi$ and $\tau^+\nu_\tau$ final states are fixed according to their known branching fractions [29].

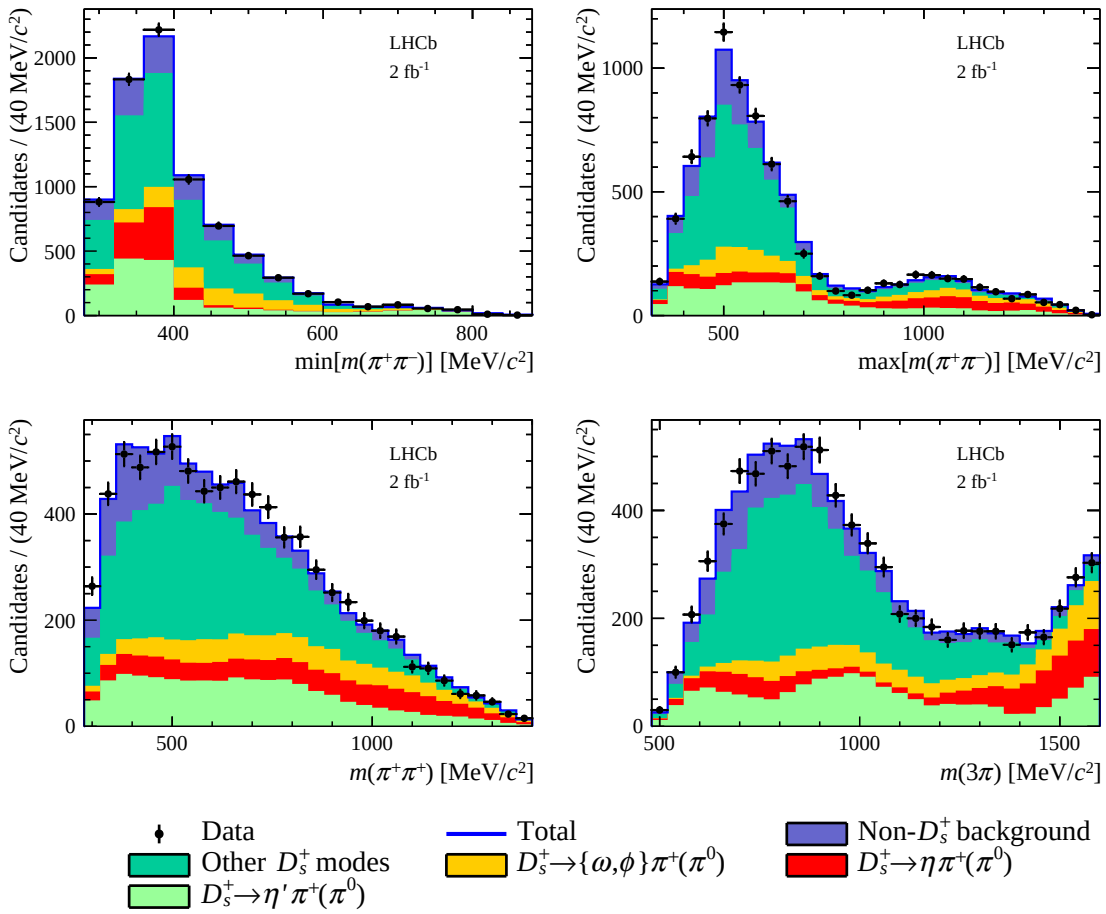


**Figure 2:** Projections of the $D_s^+ \to 3\pi X$ components for the variables: $\min[m(\pi^+\pi^-)]$, $\max[m(\pi^+\pi^-)]$, $m(\pi^+\pi^+)$ and $m(3\pi)$ in the fit to the control data samples.

The $\chi^2$ per degree of freedom is evaluated to be 1.5, indicating a reasonable fit quality. The determined fractions of the different modes are given in Table 1. They are used to correct the corresponding modes in the simulation sample. The effect of the correlations is investigated using a set of pseudodata samples built via bootstrapping from simulation, in which events are assigned to each component category randomly. The statistical uncertainty on the fit parameters is found to be underestimated by no more than 40%. The uncertainties of the fit parameters are then corrected according to this estimation. The correction factors are applied to the simulation samples that are used to produce the template PDFs for $B \to D^{*-}D_s^+X$ backgrounds.

A control sample is selected in which the $D_s^+$ decays to $\pi^+\pi^-\pi^+$ in order to determine the relative abundance of the various channels contributing to the production of a $D_s^+$ in the final state: $B^0 \to D^{*-}D_s^{(*,**)+}$ decays, and the inclusive $B \to \overline{D}^{**}D_s^+(X)$ and $B_s^0 \to D^{*-}D_s^+(X)$ decays.[1] An extended binned maximum-likelihood fit is performed to the distribution of the difference of the $D^{*-}3\pi$ mass and the sum of the reconstructed $\overline{D}^0$ and $3\pi$ masses, *i.e.* $\Delta M_{D^*D_s} \equiv m(D^{*-}3\pi) - m(\overline{D}^0) - m(3\pi)$.

[1]Throughout the paper, $\overline{D}^{**}$ and $D_s^{**+}$ are used to refer to any higher-mass excited charm or charm-strange mesons that decay into the ground-state $D^{*-}$ and $D_s^+$ meson.

**Table 1:** Relative fractions of various $D_s^+ \to 3\pi X$ decays obtained from the fit to the $D_s^+$ control sample (see Fig. 2) before applying any bias correction to the mean value of its uncertainty.

| Template | $D_s^+ \to 3\pi X$ fraction |
|---|---|
| $\eta\rho^+$ | $0.112 \pm 0.020$ |
| $\eta\pi^+$ | $0.021 \pm 0.008$ |
| $\eta'\rho^+$ | $0.185 \pm 0.016$ |
| $\eta'\pi^+$ | $0.051 \pm 0.014$ |
| $\omega\rho^+$ or $\phi\rho^+$ | $0.090 \pm 0.029$ |
| $\omega\pi^+$ or $\phi\pi^+$ | $0.041 \pm 0.008$ |
| $\eta 3\pi$ | $0.081 \pm 0.024$ |
| $\eta' 3\pi$ | $0.000 \pm 0.005$ |
| $\omega 3\pi$ | $0.032 \pm 0.041$ |
| $\phi 3\pi$ | $0.029 \pm 0.008$ |
| $K^0 3\pi$ | $0.011 \pm 0.003$ |
| $\tau^+\nu_\tau$ | $0.012 \pm 0.003$ |
| Non-resonant $3\pi$ | $0.326 \pm 0.046$ |
| $a_1\eta$ | $0.005 \pm 0.001$ |
| $a_1\eta'$ | $0.000 \pm 0.001$ |
| $a_1\omega$ | $0.002 \pm 0.002$ |
| $a_1\phi$ | $0.002 \pm 0.001$ |
| $a_1 K^0$ | $0.001 \pm 0.001$ |

**Table 2:** Decay fractions for $B \to D^{*-}D_s^+(X)$ decays obtained from data control samples. The fractions are normalised relative to that of the $B^0 \to D^{*-}D_s^{*+}$ decay. $\epsilon_{\rm control}$ is the efficiency in the control sample.

| Parameter | Fit result | $(\frac{\epsilon_{\rm sig}}{\epsilon_{\rm control}})$ | Corrected fraction |
|---|---|---|---|
| $f_{D_s^+}$ | $0.55 \pm 0.03$ | 0.992 | $0.55 \pm 0.03$ |
| $f_{D_{s0}^{*+}}$ | $0.10 \pm 0.04$ | 1.077 | $0.11 \pm 0.04$ |
| $f_{D_{s1}^+}$ | $0.37 \pm 0.07$ | 1.051 | $0.39 \pm 0.07$ |
| $f_{\bar{D}^{**}D_s^+(X)}$ | $0.28 \pm 0.10$ | 1.208 | $0.34 \pm 0.12$ |
| $f_{B_s^0 \to D^{*-}D_s^+(X)}$ | $0.12 \pm 0.04$ | 0.904 | $0.11 \pm 0.04$ |

The distributions of $\Delta M_{D^*D_s}$, $q^2$, decay time of the $\tau^+$ candidate ($t_\tau$) and anti-$D_s^+$ BDT output are shown in Fig. 3. The fit quality is good with a $\chi^2$ per degree of freedom equalling 1.11. The fractions of different decays are given in Table 2, which are used as Gaussian constraints in the signal-extraction fit for the corresponding components after accounting for the efficiency differences between the control and signal samples.

The $B \to D^{*-}D^+(X)$ and $B \to D^{*-}D^0(X)$ decays are the sub-leading double-charm backgrounds in the signal sample, where the $D^0$ and the $D^+$ mesons decay to three charged pions plus extra particles. A control sample representing the $B \to D^{*-}D^0X$ decays is selected using the decay mode $D^0 \to K^-3\pi$. This control samples is used to check the agreement with simulation for the signal fit variables $q^2$, $t_\tau$ and anti-$D_s^+$ BDT output. The $q^2$ distribution shows disagreement

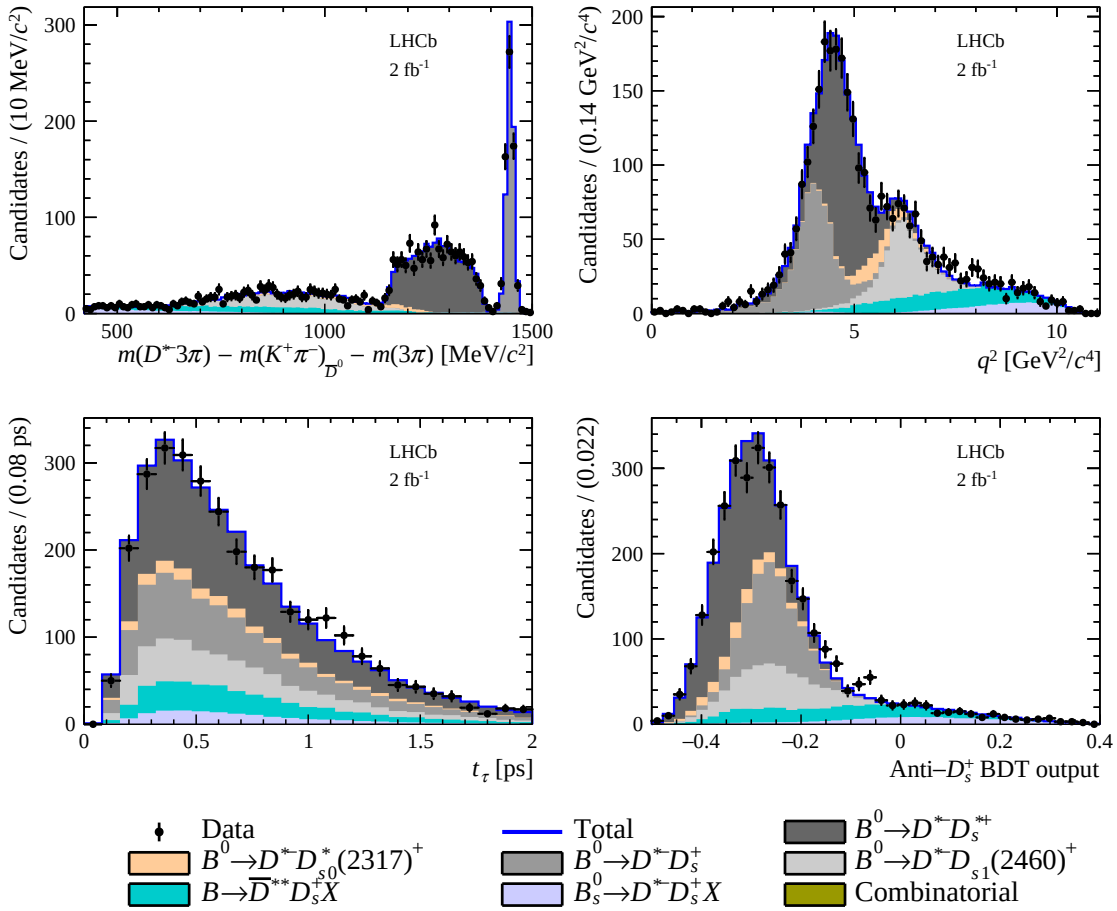


**Figure 3:** Distributions of $\Delta M_{D^*D_s}$, $q^2$, $t_\tau$ and anti-$D_s^+$ BDT output for the $B \to D^{*-}D_s^+(X)$ components. The results of the fit are overlaid.

between data and simulation due to the imperfect modelling of inclusive $3\pi$ decays. Therefore, the simulation is corrected to match the data distributions. Fig. 4 shows the $q^2$ distributions before and after the correction. The agreement is good in the case of the other two fit variables, $t_\tau$ and anti-$D_s^+$ BDT output, and no further correction is necessary.

### 4.3 Determination of the signal and normalisation yields

The $B^0 \to D^{*-}\tau^+\nu_\tau$ yield is determined from an extended binned maximum-likelihood fit to the distributions of $q^2$, $t_\tau$ and anti-$D_s^+$ BDT output. The binning scheme comprises eight bins in $q^2$ and $t_\tau$, and six bins in the BDT output. The chosen binning scheme has maximum sensitivity to $B^0 \to D^{*-}\tau^+\nu_\tau$ yield while still sufficiently populating the bins. The ranges of $q^2$, $t_\tau$ and BDT distributions are $[0, 11]$ GeV$^2/c^4$, $[0, 2]$ ps and $[-0.2, 0.5]$, respectively. The fit model is built as a three-dimensional template. The templates for the combinatorial components are derived from data in which same-sign combinations of $D^*$ and $\tau$ candidates are selected, whereas the remainder are obtained from simulation.

The fit results are summarised in Table 3 and the distributions of the fit variables are shown in Fig. 5. The fit is performed in two iterations: first, the fractions of $D^0$ are varied freely and the six

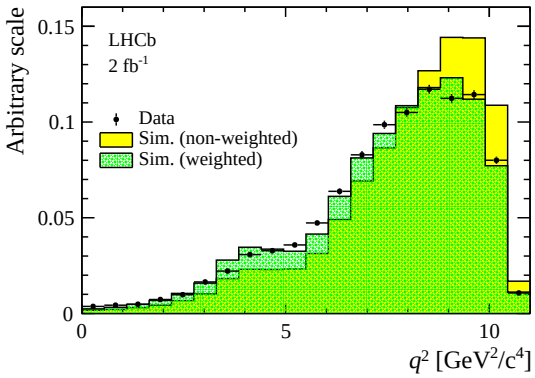


**Figure 4:** Simulated $q^2$ distributions for $B \to D^{*-}D^0(X)$ before and after weighting based on the data control samples.

$D_s^+$ decay modes are Gaussian constrained, and then a second fit is performed by fixing these to their best fit values. This is the same strategy followed in Refs. [6] to determine the statistical uncertainty on the $B^0 \to D^{*-}\tau^+\nu_\tau$ yield. Thus the relative statistical precision on the yield changes from 6.2% to 5.9%. The quadratic difference between the statistical uncertainties in the two iterations is treated as a systematic uncertainty from the double-charm decay models. The number of signal events is determined to be $2469 \pm 154$, where the uncertainty is statistical only. The fit quality is excellent with a $\chi^2$ per degree of freedom of 1.0. From studies using pseudoexperiments, the fit is found to be unbiased.

The $B^0 \to D^{*-}3\pi$ yield is estimated from an unbinned maximum-likelihood fit to the $D^{*-}3\pi^\pm$ mass distribution. The signal model consists of a Crystal Ball (CB) function [31] and two Gaussian functions that share a common mean. The CB shape parameters, the width of the wider Gaussian and the relative proportion of the two Gaussian functions are fixed to the values obtained from simulation. The background component is described by an exponential function. The $m(D^{*-}3\pi)$ distribution is shown in Fig. 6 (left) with the fit projection overlaid. The data sample contains $B^0 \to D^{*-}D_s^+(\to 3\pi)$ decays, which must be subtracted from the $B^0 \to D^{*-}3\pi$ yield (Fig. 6, right). A fit to the $m(3\pi)$ distribution in the mass range $1800 - 2100\,\mathrm{MeV}/c^2$ yields $451 \pm 35$ decays. After the subtraction, there are $30540 \pm 182$ $B^0 \to D^{*-}3\pi$ decays. Here, the uncertainties are statistical only.

The $B^0 \to D^{*-}\tau^+\nu_\tau$ and $B^0 \to D^{*-}3\pi$ yields and their efficiencies are used to determine $\mathcal{K}(D^{*-})$, yielding a result of $1.70 \pm 0.10^{+0.11}_{-0.10}$, where the uncertainties are statistical and systematic, respectively.

### 4.4 Systematic uncertainties

The complete study of systematic uncertainties is detailed in Ref. [27]. The table 4 summarizes the contribution of the various sources. The dominant ones are coming from the limited knowledge of signal and background template shapes, and limited simulation statistics. The uncertainty related to the external branching fractions for $B^0 \to D^{*-}\mu^+\nu_\mu$ and $B^0 \to D^{*-}\pi^+\pi^-\pi^+$ need to be added for the measurement of $\mathrm{R}(D^{*\pm})$.

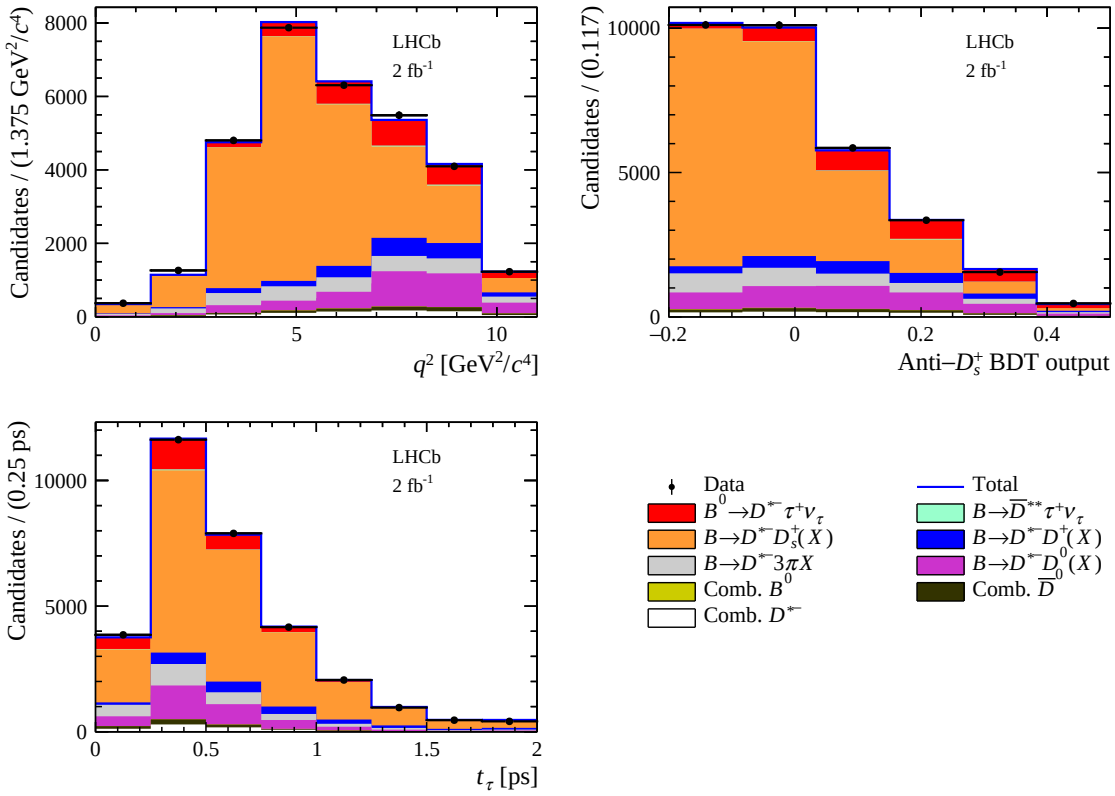


**Figure 5:** Distributions of the fit variables in the $B^0 \to D^{*-}\tau^+\nu_\tau$ data sample with the fit result overlaid.

### 4.5 Conclusion

In conclusion, using $pp$ collision data collected in 2015 and 2016 by the LHCb experiment and corresponding to an integrated luminosity of 2 fb$^{-1}$, the ratio of branching fractions of $B^0 \to D^{*-}\tau^+\nu_\tau$ and $B^0 \to D^{*-}3\pi$ decays is measured as

$$\mathcal{K}(D^{*-}) = 1.70 \pm 0.10(\text{stat})^{+0.11}_{-0.10}(\text{syst})\,.$$

The result is in good agreement with the previous LHCb measurement [5, 6]. The improved analysis procedure results in an increase in signal efficiency and a decrease of the relative systematic uncertainty from 9% to 6%. Using the most recent branching fraction measurements $\mathcal{B}(B^0 \to D^{*-}3\pi) = (7.21 \pm 0.29) \times 10^{-3}$ and $\mathcal{B}(B^0 \to D^{*-}\mu^+\nu_\mu) = (4.97 \pm 0.12)\%$ [29], the branching fraction

$$\mathcal{B}(B^0 \to D^{*-}\tau^+\nu_\tau) = (1.23 \pm 0.07\,(\text{stat})^{+0.08}_{-0.07}\,(\text{syst}) \pm 0.05\ (\text{ext})) \times 10^{-2}\,,$$

and the ratio of branching fractions of $B^0 \to D^{*-}\tau^+\nu_\tau$ and $B^0 \to D^{*-}\mu^+\nu_\mu$

$$\mathcal{R}(D^{*-}) = 0.247 \pm 0.015\,(\text{stat}) \pm 0.015\,(\text{syst}) \pm 0.012\ (\text{ext})\,,$$

are obtained, where the third uncertainties are due to the uncertainties on the external branching fractions. This result is compatible with the present world average and with the SM expectation

**Table 3:** Fit results from the three-dimensional signal-extraction fit to $q^2$, $t_\tau$ and anti-$D_s^+$ BDT output in the data.

| Parameter | Fit result | Constraint |
|---|---|---|
| | Free | |
| $N_{\rm sig}$ | 2469 ± 154 | |
| $N_{D_s^+}$ | 20446 ± 509 | |
| $f_{D^+}$ | 0.08 ± 0.01 | |
| $f_{D^0}^{\nu_1\nu_2}$ | 2.10 ± 0.30 | |
| | Constrained | |
| $N_{B\to D^{*-}3\pi X}$ | 2279 ± 177 | 2051 ± 200 |
| $f_{B_s^0\to D^{*-}D_s^+(X)}$ | 0.13 ± 0.03 | 0.11 ± 0.04 |
| $f_{D_{s1}^+}$ | 0.36 ± 0.03 | 0.40 ± 0.07 |
| $f_{D_s^+}$ | 0.60 ± 0.02 | 0.55 ± 0.03 |
| $f_{D_{s0}^{*+}}$ | 0.06 ± 0.03 | 0.11 ± 0.04 |
| $f_{\overline{D}^{**}D_s^+(X)}$ | 0.61 ± 0.06 | 0.34 ± 0.12 |
| | Fixed | |
| $N_{B_1B_2}$ | 46 | |
| $N_{D^0}^{\rm same}$ | 1051 | |
| $N_{\rm fake\ \overline{D}^0}$ | 468 | |
| $N_{\rm fake\ D^{*-}}$ | 714 | |
| $f_{\overline{D}^{**}\tau^+\nu}$ | 0.035 | |
| $f_{\tau^+\to 3\pi\overline{\nu}_\tau}$ | 0.780 | |

(0.254 ± 0.005) [8]. When combined with the previous results [6], the values of $\mathcal{K}(D^{*-})$ and $\mathcal{R}(D^{*-})$ are

$$\mathcal{K}(D^{*-})_{\rm comb} = 1.77 \pm 0.08\,({\rm stat}) \pm 0.10\,({\rm syst})\ {\rm and}$$
$$\mathcal{R}(D^{*-})_{\rm comb} = 0.257 \pm 0.012\,({\rm stat}) \pm 0.014\,({\rm syst}) \pm 0.012\ ({\rm ext})\,.$$

The combined $\mathcal{R}(D^{*-})$ is obtained from the $\mathcal{K}(D^{*-})$ combination and the branching fractions of the normalisation channels. This combination leads to one of the most precise measurements of $\mathcal{R}(D^*)$ to date. The combination of all R($D^*$) and R(D) measurements to date, including a very recent measurement by the BELLE-II collaboration, is displayed on Fig.7 [8]. It shows a 3.3 deviation from the SM prediction. Ten years after the first BABAR measurement, and after a dozen of various measurements, it is interesting (and may be frustrating as well!) to note that the discrepancy level wrt to SM predictions is still the same (!), although of course both theoretical and experimental uncertainties have been significantly reduced. As we say in France, *"Le canard est toujours vivant..."*.

## 5. $D^{*-}$ polarization measurement

This section is based on a forthcoming LHCb publication [32] in preparation. The results in this section are therefore to be considered as preliminary.

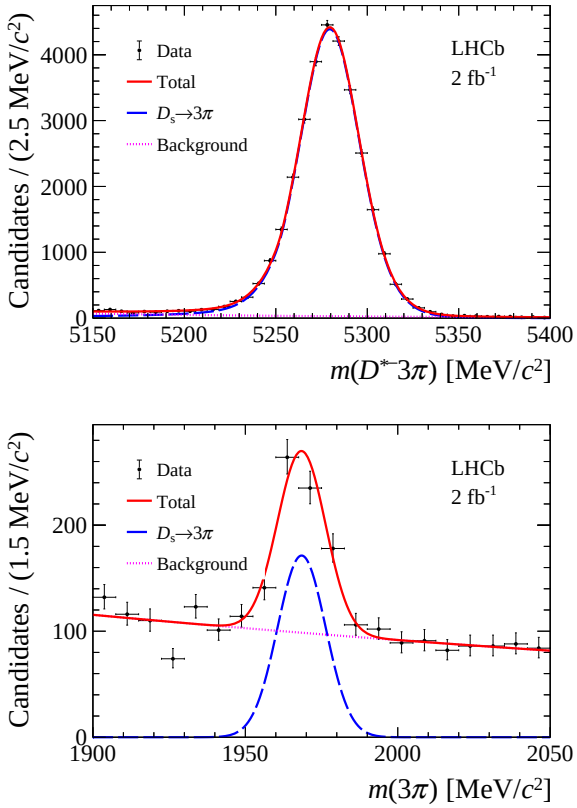


**Figure 6:** Invariant-mass distribution of the (left) $D^{*-}3\pi$ and (right) $3\pi$ system for $B^0 \to D^{*-}3\pi$ candidates in data with corresponding fit models superimposed.

### 5.1 Introduction

Studies of the kinematic and angular distributions, such as the longitudinal $D^*$ polarization fraction ($F_L^{D^*}$), can provide additional sensitivity to possible NP scenarios even if R($D^*$) is fully compatible with the SM prediction [33]. For example, the $F_L^{D^*}$ value could be enhanced by new scalar operators or suppressed by new tensor operators [34]. At present, the only measurement of $F_L^{D^*}$ was performed by the Belle collaboration with the result $F_L^{D^*} = 0.60 \pm 0.08$ (stat) $\pm 0.04$ (syst) [35]. This value is compatible with the SM expectation [36–38]. The most recent theoretical predictions, computed with different model assumptions and QCD calculations, are 0.441 $\pm$ 0.006 [39], 0.457 $\pm$ 0.010 [40] and 0.467 $\pm$ 0.009 [41].

The polarization measurement is performed including the data collected by the LHCb experiment during 2011–2012 at $\sqrt{s}$ equal to 7 and 8 TeV (Run 1) and during the 2015–2016 (Run 2) at $\sqrt{s}$ = 13 TeV, corresponding to an integrated luminosity of 3 fb$^{-1}$ and 2 fb$^{-1}$, respectively. The event selection requirements are exactly the same as the ones described above for the R($D^{*\pm}$) analysis. The value of the $F_L^{D^*}$ observable is extracted from the angular distribution of the $D^{*-} \to \overline{D}{}^0\pi^-$ decay:

$$\frac{d^2\Gamma}{dq^2 d\cos\theta_D} = a_{\theta_D}(q^2) + c_{\theta_D}(q^2)\cos^2\theta_D, \qquad (1)$$

**Table 4:** Summary of relative systematic uncertainties on the ratio $\mathcal{K}(D^{*-})$.

| Source | systematic uncertainty (%) |
|---|---|
| Signal decay template shape | 1.8 |
| Signal decay efficiency | 0.9 |
| Fractions of signal $\tau^+$ decays | 0.3 |
| Possible contributions from other $\tau^+$ decays | 1.0 |
| Fixing the $\overline{D}^{**}\tau^+\nu_\tau$ and $D_s^{**+}\tau^+\nu_\tau$ fractions | $^{+1.8}_{-1.9}$ |
| Normalisation mode PDF choice | 1.0 |
| Knowledge of the $D_s^+ \to 3\pi X$ decay model | 1.0 |
| Specifically the $D_s^+ \to a_1 X$ fraction | 1.5 |
| $B \to D^{*-}D_s^+(X)$ template shapes | 0.3 |
| $B \to D^{*-}D^0(X)$ template shapes | 1.2 |
| $B \to D^{*-}D^+(X)$ template shapes | $^{+2.2}_{-0.8}$ |
| Fixing $B \to D^{*-}D_s^+(X)$ bkg model parameters | 1.1 |
| Fixing $B \to D^{*-}D^0(X)$ bkg model parameters | 1.5 |
| $B \to D^{*-}3\pi X$ template shapes | 1.2 |
| Combinatorial background normalisation | $^{+0.5}_{-0.6}$ |
| PID efficiency | 0.5 |
| Kinematic reweighting | 0.7 |
| Vertex error correction | 0.9 |
| Normalisation mode efficiency (modelling of $m(3\pi)$) | 1.0 |
| Preselection efficiency | 2.0 |
| Signal efficiency (size of simulation sample) | 1.1 |
| Normalisation efficiency (size of simulation sample) | 1.1 |
| Empty bins in templates | 1.3 |
| PDF shapes uncertainty (size of simulation sample) | 2.0 |
| Total systematic uncertainty | $^{+6.2}_{-5.9}$ |
| Total statistical uncertainty | 5.9 |

where $\theta_D$ is the angle between the $\overline{D}^0$ meson direction and the direction opposite to the $B^0$ in the $D^*$ rest frame, $q^2$ is the squared invariant mass of the $\tau\nu_\tau$ system, defined as the squared difference between the $B$ and the $D^*$ momentum, and the $a_{\theta_D}(q^2)$ and $c_{\theta_D}(q^2)$ coefficients are linear combinations of the 12 angular coefficients, encapsulating the hadronic effects and the fundamental couplings [42]. The $q^2$ computation is performed correcting the $B$ momentum for the missing neutrino effect. The value of $F_L^{D^*}$ can be calculated as:

$$F_L^{D^*} = \frac{a_{\theta_D}(q^2) + c_{\theta_D}(q^2)}{3a_{\theta_D}(q^2) + c_{\theta_D}(q^2)}. \tag{2}$$

### 5.2 Polarization measurements

The final $F_L^{D^*}$ value is calculated from the $a_{\theta_D}(q^2)$ and $c_{\theta_D}(q^2)$ parameters extracted from a binned maximum-likelihood fit to data. The fit uses four-dimensional templates in terms of the

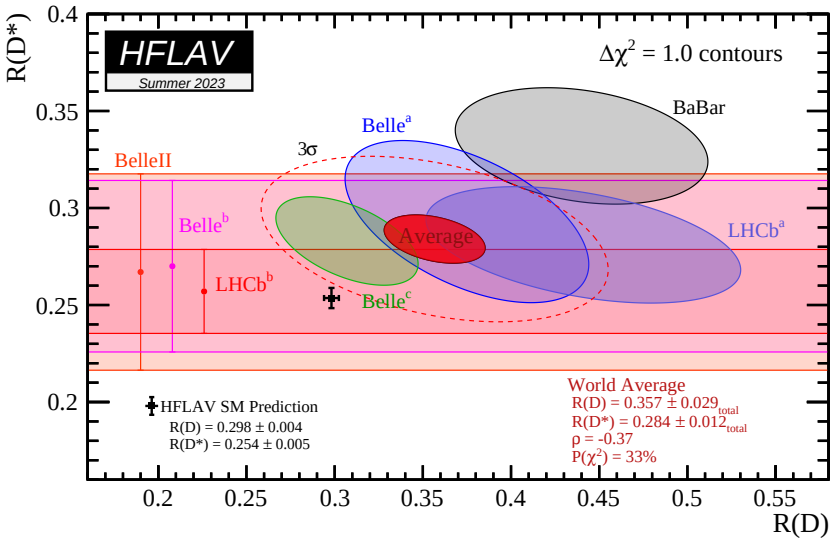


**Figure 7:** HFLAV compilation (Summer 2023) of all the results regarding R($D^*$) and R(D).

following variables:

- $\cos\theta_D$: defined in Section 5.1;
- $q^2$: defined in Section 5.1;
- $t_\tau$: decay-time of the $\tau$ lepton, taking into account the corrections due to the missing neutrino;
- anti-$D_s^+$ BDT: the output of the BDT trained to suppress the $B \to D^{*-}D_s^+(X)$ background.

The value of $F_L^{D^*}$ is measured in two different $q^2$ regions, below and above 7 GeV$^2/c^4$, and considering 6 bins of $\cos\theta_D$ in each region. The binning scheme for the other two variables differs for the Run 1 and Run 2 samples, due to their different luminosities. Within the $t_\tau$ in range [0, 2] ps there are four and six bins for the Run 1 and Run 2 datasets, respectively. Similarly, either six or eight bins are used for the anti-$D_s^+$ BDT distribution.

The $a_{\theta_D}(q^2)$ and $c_{\theta_D}(q^2)$ parameters are determined by splitting the signal simulated template in two components: one is completely unpolarized while the other is fully polarized, allowing to determine a different $F_L^{D^*}$ value from the one used in the simulated signal sample generation. With this separation, the $a_{\theta_D}(q^2)$ and $c_{\theta_D}(q^2)$ parameters become directly proportional to the yields of the unpolarized and polarized components, respectively, as discussed in Section 5.6.

Weights are assigned to the simulated events such that the decay kinematics follow the CLN parameterization of the form factors [43]. This procedure is performed by means of the Hammer tool [44] using the dedicated RooHammerModel [45] interface developed by the LHCb collaboration.

A correction to the signal $\cos\theta_D$ distribution is implemented in order to take into account possible effects due to the reconstruction of the signal decays and retrieve the correct $F_L^{D^*}$ value. This correction consists of two contributions: the first corrects for the effect of the signal selection chain and the second corrects for the bin migration due to differences between the true and

reconstructed variables. The former is determined as the ratio of the true $\cos\theta_D$ distribution, after the full signal selection, to the corresponding distribution at generation level in bins of true $q^2$; the latter is determined as the ratio between the $\cos\theta_D$ distribution in bins of $q^2$ considering the reconstructed and the generated quantities, after the full signal selection. The ratio between these $\cos\theta_D$ distributions is computed with the non-uniform distribution of the events in each bin taken into account.

The signal $\cos\theta_D$ distribution in the two $q^2$ regions for the unpolarized and polarized components, after applying the full signal selection and the form-factor and correction weights, is depicted in Figure 8. The unpolarized component does not exhibit a flat distribution since it is distorted by reconstruction effects.

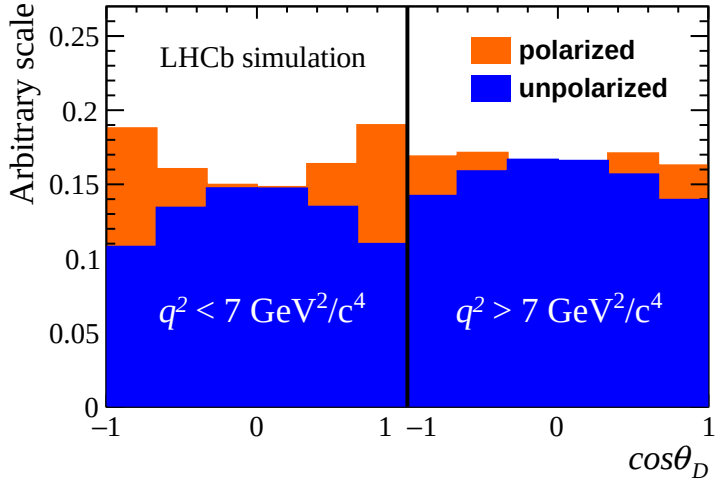


**Figure 8:** Signal distribution of the $\cos\theta_D$ variable in the two $q^2$ regions and split into the unpolarized and polarized components. The template for the unpolarized component is distorted by the effect of the reconstruction and the signal selection.

### 5.3 Background description

After applying the signal selection, the residual background consists mainly of events with a charm hadron decay: $B \to D^{*-}D(X)$ decays, where $D$ can be, in order of importance, a $D_s^+$, a $D^+$ or a $D^0$ meson. Probability density functions (PDFs) for these background sources are extracted from simulated control samples. The corresponding distributions in Run 1 and Run 2 data are used to validate the simulated samples and, if needed, calculate corrections to be applied to the simulation. Two different control samples are used to validate the simulated $D_s^+$ background: the first is based on a pure sample of $D_s^+$ decaying into three charged pions aimed to correct the branching fractions leading to $D_s^+$ meson production in the generation phase; the second consisting of various $B \to D^{*-}D_s^+(X)$ decays aims to constrain the relative fractions between these components in the final fit.

### 5.4 $B \to D^{*-}(D^+, D^0)(X)$ control sample

The decays $B \to D^{*-}D^+(X)$ and $B \to D^{*-}D^0(X)$ can contribute to the signal background when the $D^+$ meson decays into two charged pions and a kaon, misidentified as a pion, or when

a $D^+$ or $D^0$ meson decays into three charged pions and an additional particle. The corresponding simulated samples are used to extract the PDFs for the four fit variables and a validation of their shape is performed using dedicated control samples. For the latter background, a control sample is built by reconstructing the $D^0 \to K^-\pi^+\pi^-\pi^+$ decay by means of the isolation algorithm, searching for the extra kaon around the $3\pi$ vertex. For the former background, a control sample is obtained by inverting the PID requirement on the negative charged pion and reconstructing the $D^+ \to K^-\pi^+\pi^+$ decay. In both cases a *sPlot* [46] is performed to get rid of the combinatorial background and obtain a pure distribution of the decay mode of interest. The $q^2$ distribution shows some discrepancies between data and simulation due to the imperfect modelling of the inclusive $3\pi$ decays. A correction is determined as the ratio of the data and simulated $q^2$ distributions and is applied to the final templates to account for this effect. Similarly, the $\cos\theta_D$ distribution is not well modelled in the inclusive simulation and is therefore corrected in order to match the one observed in data. The data and simulated $q^2$ and $\cos\theta_D$ distributions before and after the corrections for the $B \to D^{*-}D^0(X)$ decays are depicted in Figure 9.

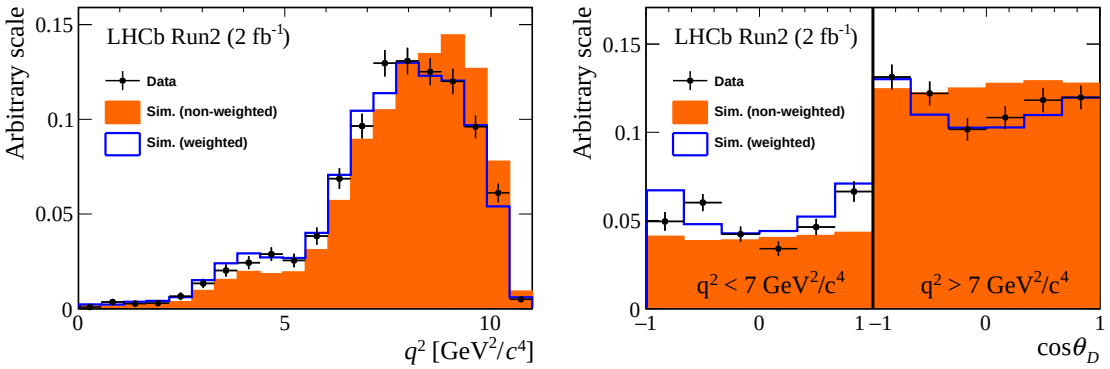


**Figure 9:** Simulated (left) $q^2$ and (right) $\cos\theta_D$ distributions for the $B \to D^{*-}D^0(X)$ before and after the correction for the data-simulation differences in the Run 2 sweighted data sample.

### 5.5 Signal fit

The fraction of signal polarized events is estimated from an extended maximum-likelihood fit to the four dimensional distribution of $\cos\theta_D$, $q^2$, $t_\tau$, anti-$D_s^+$ BDT output. The fit is performed within the SM framework with the free parameters listed below.

- $N^{\text{unpol}}_{\text{low } q^2}$ and $N^{\text{unpol}}_{\text{high } q^2}$: parameters accounting for the number of unpolarized signal events in the low and high $q^2$ regions, respectively.
- $f^{\text{pol}}_{\text{low } q^2}$ and $f^{\text{pol}}_{\text{high } q^2}$: parameters accounting for the fraction of signal polarized events with respect to the number of unpolarized signal events in the low and high $q^2$ regions, respectively.
- $N_{B^0 \to D^{*-}D^+(X)}$: parameter accounting for the number of $B^0 \to D^{*-}D^+(X)$ events.
- $f^{\nu_1\nu_2}_{B^0 \to D^{*-}D^0(X)}$: free parameter accounting for the fraction of $B^0 \to D^{*-}D^0(X)$ events where at least one pion comes from a different vertex than the $D^0$ vertex, with respect to $N^{\text{same}}_{B^0 \to D^{*-}D^0(X)}$.

- $N_{B^0 \to D^{*-} D_s^{*+}}$: parameter accounting for the yield of the $B^0 \to D^{*-} D_s^{*+}$ mode.

In order to reach a better fit convergence some parameters have been contrained or fixed:

- $f_{\tau^+ \to \pi^+\pi^-\pi^+\pi^0\nu_\tau}$: fraction of signal $\tau^+ \to \pi^+\pi^-\pi^+\pi^0\nu_\tau$ events with respect to $\tau^+ \to \pi^+\pi^-\pi^+\nu_\tau$. This parameter is fixed taking into account the different branching ratios and efficiencies of the two modes.

- $f_{B^0 \to D^{**-}\tau^+\nu_\tau}$: fraction of signal $B^0 \to D^{**-}\tau^+\nu_\tau$ with respect to $B^0 \to D^{*-}\tau^+\nu_\tau$. This parameter is fixed in the fit to the expected value determined from simulation.

- $f_{B^0 \to D^{*-} D_{s1}^{\prime +}}$, $f_{B^0 \to D^{*-} D_s^+}$, $f_{B^{0,\pm} \to D^* D_s^+ X}$, $f_{B_s^0 \to D^{*-} D_s^+(X)}$ and $f_{B^0 \to D^{*-} D_{s0}^{*+}}$: set of parameters representing the fraction of a decay mode of interest with respect to the $B^0 \to D^{*-} D_s^{*+}$ decay. These parameters are constrained to the results of the fit performed in Section 5.3 after correcting for efficiency.

- $N^{\text{same}}_{B^0 \to D^{*-} D^0(X)}$: number of $B^0 \to D^{*-} D^0(X)$ events where the three pions in the final state come from the same vertex. This parameter is Gaussian constrained to the number of exclusive $D^0 \to K^-\pi^+\pi^-\pi^+$ events recovered by the isolation tool after correcting for the data-simulation differences.

- $N_{B^0 \to D^{*-}\pi^+\pi^-\pi^+ X}$: constrained parameter accounting for the number of prompt $B^0 \to D^{*-}\pi^+\pi^-\pi^+ X$ events. The central value is determined from the observed ratio between exclusive $B^0 \to D^{*-}\pi^+\pi^-\pi^+$ and the inclusive $B^0 \to D^{*-}\pi^+\pi^-\pi^+ X$ decays, corrected for data-simulation differences.

- $N_{\text{B1-B2}}$: number of combinatorial backgrounds where the $D^*$ and the three pions come from different $B$ hadrons. Its value is fixed to the value observed in the wrong-sign sample satisfying the non-isolation and the higher $B$ mass requirements.

- $N_{\text{fake } D^0}$ & $N_{\text{fake } D^*}$, number of combinatorial background events where a fake $D^0$ or $D^*$ is reconstructed, respectively. Their value is fixed to the values obtained from a fit to $m(K^-\pi^+)$ and $m(D^*) - m(K^-\pi^+)$.

The fractions $f^{\text{pol}}$, $f_{\tau^+ \to \pi^+\pi^-\pi^+\pi^0\nu_\tau}$ and $f_{B^0 \to D^{**-}\tau^+\nu_\tau}$ are assumed to be the same in the Run 1 and Run 2 data samples. The fit has a $\chi^2$ for degree of freedom of 1.1 (806/736), the results are summarized in Table 5 while the fit variable projections are depicted in Figure 10. The fractions of polarized signal events are $0.361 \pm 0.074$ and $0.013 \pm 0.081$ for the low and high $q^2$ region, respectively.

### 5.6 Extraction of the $D^*$ polarization

The $a_{\theta_D}(q^2)$ and $c_{\theta_D}(q^2)$ coefficients are directly related to the observed yields of the polarized and unpolarized signal components in the two $q^2$ bins. In fact, the $a_{\theta_D}(q^2)$ value can be computed as the value of the unpolarized PDF evaluated at $\cos\theta_D = 0$ scaled by the number of unpolarized events, while the $c_{\theta_D}(q^2)$ parameter is proportional to the integral of the polarized PDF. The corresponding $F_L^{D^*}$ value integrated over the whole $q^2$ region is determined as the average of the two $F_L^{D^*}$ values, corrected by efficiency. The extracted $F_L^{D^*}$, $a_{\theta_D}(q^2)$ and $c_{\theta_D}(q^2)$ values for the binned and integrated $q^2$ regions are reported in Table 6.

**Table 5:** Fit results of the nominal fit for the Run 1 and Run 2 datasets.

| Parameter | Run 1 | Run 2 |
|---|---|---|
| $N^{\text{unpol}}_{\text{low } q^2}$ | 360 ± 55 | 758 ± 62 |
| $N^{\text{unpol}}_{\text{high } q^2}$ | 532 ± 70 | 827 ± 109 |
| $f^{\text{pol}}_{\text{low } q^2}$ | 0.36 ± 0.07 | |
| $f^{\text{pol}}_{\text{high } q^2}$ | 0.01 ± 0.08 | |
| $f_{\tau^+\to\pi^+\pi^-\pi^+\pi^0\nu_\tau}$ | 0.28 | |
| $f_{B^0\to D^{**-}\tau^+\nu_\tau}$ | 0.044 | |
| $N_{B^0\to D^{*-}D_s^{*+}}$ | 2087 ± 77 | 7475 ± 170 |
| $f_{B^0\to D^{*-}D_{s1}'^+}$ | 0.38 ± 0.05 | 0.37 ± 0.04 |
| $f_{B^0\to D^{*-}D_s^+}$ | 0.51 ± 0.03 | 0.60 ± 0.03 |
| $f_{B^{0,\pm}\to D^* D_s^+ X}$ | 0.83 ± 0.06 | 0.48 ± 0.05 |
| $f_{B_s^0\to D^{*-}D_s^+(X)}$ | 0.17 ± 0.03 | 0.10 ± 0.02 |
| $f_{B^0\to D^{*-}D_{s0}^{*+}}$ | 0.11 ± 0.02 | 0.02 ± 0.03 |
| $N^{\text{same}}_{B^0\to D^{*-}D^0(X)}$ | 448 ± 22 | 1039 ± 52 |
| $f^{\nu_1\nu_2}_{B^0\to D^{*-}D^0(X)}$ | 0.39 ± 0.18 | 2.26 ± 0.28 |
| $N_{B^0\to D^{*-}D^+(X)}$ | 1747 ± 118 | 1740 ± 182 |
| $N_{B^0\to D^{*-}\pi^+\pi^-\pi^+X}$ | 408 ± 21 | 2190 ± 33 |
| $N_{\text{B1}-\text{B2}}$ | 197 | 216 |
| $N_{\text{fake } D^0}$ | 110 | 457 |
| $N_{\text{fake } D^*}$ | 133 | 533 |

**Table 6:** Values of $a_{\theta_D}(q^2)$, $c_{\theta_D}(q^2)$ and $F_L^{D^*}$ from the fit.

| Parameter | $q^2 < 7\,\text{GeV}^2/c^4$ | $q^2 > 7\,\text{GeV}^2/c^4$ | integrated |
|---|---|---|---|
| $a_{\theta_D}(q^2)$ | 0.12 ± 0.02 | 0.15 ± 0.03 | 0.14 ± 0.03 |
| $c_{\theta_D}(q^2)$ | 0.13 ± 0.05 | 0.01 ± 0.02 | 0.07 ± 0.06 |
| $F_L^{D^*}$ | 0.51 ± 0.07 | 0.35 ± 0.08 | 0.43 ± 0.06 |

### 5.7 Systematic uncertainties

Different sources of systematic uncertainty are considered, mainly due to the signal selection requirements, $q^2$ bin migration, signal and background modelling, and limited size of the simulated samples. A breakdown of all the systematic uncertainties is reported in Table 7 while in the following a brief description is provided for each source.

The simulated signal distributions are weighted according to the form-factor values predicted by the CLN parameterization. Two systematic uncertainties are assigned due to limited knowledge of the form-factors: *FF parameters* is evaluated varying the CLN parameters within their uncertainties, while *FF model* is determined repeating the fit with the BGL parameterization [47, 48].

The effect of the *signal selection* and the $q^2$ *bin migration* on the signal $\cos\theta_D$ template are also considered, due to their effect on the split between polarized and unpolarized components. A systematic uncertainty is assigned varying these two latter corrections within their statistical

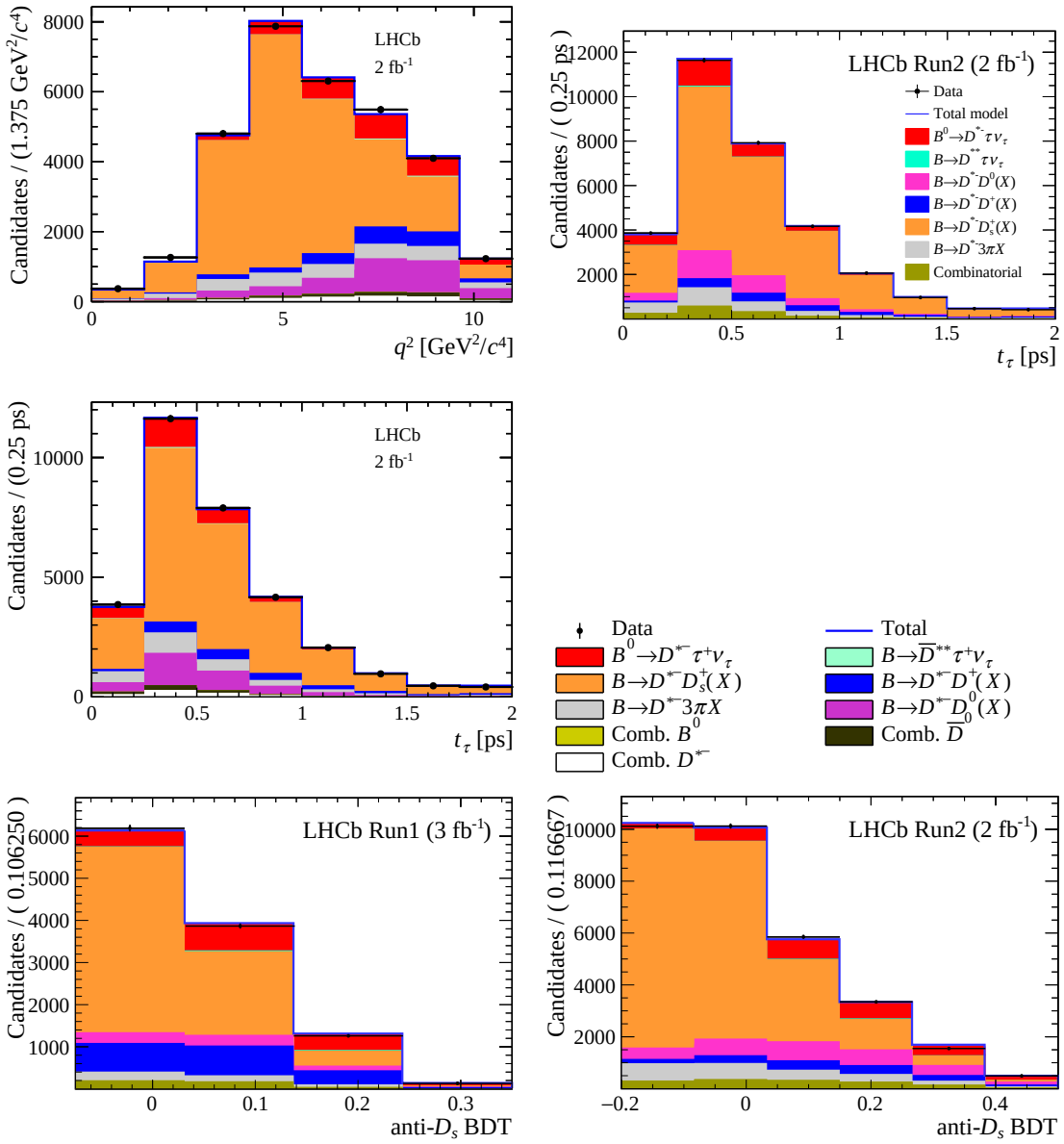


**Figure 10:** Distributions of the fit variables in the Run 1 (left) and Run 2 (right) datasets with the fit results superimposed.

uncertainties. The presence of any bias in the fit procedure is assessed repeating the fit on a set of pseudo-experiments, obtained with a bootstrap technique on data distribution, and assessing a systematic uncertainty on the resulting $F_L^{D^*}$ values (*Fit validation*). The $F_L^{D^*}$ value used in the generation of the simulated signal sample ($F_L^{D^*}$ *in simulation*) can introduce a bias in the reconstruction efficiency and acceptance in the $\cos\theta_D$ distribution. Different $F_L^{D^*}$ hypotheses are considered in the full $F_L^{D^*}$ range obtaining each time a new set of signal templates. The fit is repeated and a systematic uncertainty is assigned as the maximum difference with respect to the default $F_L^{D^*}$ values.

The fraction between the $\tau^+ \to \pi^+\pi^-\pi^+\nu_\tau$ and $\tau^+ \to \pi^+\pi^-\pi^+\pi^0\nu_\tau$ decays is fixed in the signal fit so a systematic uncertainty (*Fractions of signal $\tau^+ \to \pi^+\pi^-\pi^+\pi^0\nu_\tau$ decays*) is assigned repeating the fit and varying the central value according to its uncertainty. A similar strategy is used for the $f_{B^0 \to D^{**-}\tau^+\nu_\tau}$, constraining the ratio between the $B^0 \to D^{**-}\tau^+\nu_\tau$ events and the signal decay (*Fraction of $D^{**}$ feed-down*).

The $D_s^+$ decays in simulation are corrected by the weights obtained in the fit to the $D_s^+ \to \pi^+\pi^-\pi^+(X)$ control sample (*$D_s^+$ decay model*). These weights are varied by taking into account their uncertainties and correlations and the signal fit is repeated with the varied $D_s^+$ templates. Different corrections have been applied to the templates of double charmed backgrounds in order to obtain the data-simulation corrected $\cos\theta_D$ distributions. For each correction a systematic uncertainty is assigned by varying the corresponding weights within their uncertainty (*Shape of $\cos\theta_D$ template in $D^*D$ decays*).

Another source of systematic uncertainty is related to the limited size of the simulated events available for building the fit templates for the various components (*Limited template statistics*). This systematic uncertainty is evaluated repeating the fit using alternative templates obtained after resampling the nominal ones by means of a bootstrap technique. The usage of the ReDecay [25] technique in the generation of large simulated samples helped in taking this systematic well under control.

A different fitting strategy is implemented in order to estimate the $F_L^{D^*}$ value with an alternative method. The fit is repeated using 3D templates including the $\tau$ decay-time, the anti-$D_s^+$ BDT and $q^2$. The fit results are projected in the $\cos\theta_D$ variable and a background subtraction is performed. Finally the $\cos\theta_D$ distribution, corrected for reconstruction effects, is fitted using a second order polynomial for determining the $a_{\theta_D}(q^2)$ and $c_{\theta_D}(q^2)$ parameters. The results are found to be compatible with the nominal strategy.

An additional systematic uncertainty has been assigned for the extrapolation of the $F_L^{D^*}$ value in the whole $q^2$ integrated region. The bin efficiencies used for determining the integrated $F_L^{D^*}$ value are varied by 1 standard deviation and the difference with respect to the nominal value is taken as systematic uncertainty ($F_L^{D^*}$ *integration method*).

### 5.8 Conclusions

The measurement of the longitudinal $D^*$ polarization is performed by the LHCb collaboration using the data samples collected at the center-of-mass energy $\sqrt{s}$ equal to 7, 8 and 13 TeV corresponding to an integrated luminosity of 1, 2 and 2 fb$^{-1}$, respectively. The $F_L^{D^*}$ value is provided in two $q^2$ bins and in the integrated region. The measured $F_L^{D^*}$ values, which are compatible with SM predictions and with the results obtained by the Belle experiment, are:

$$\begin{aligned} q^2 < 7\,\mathrm{GeV}^2/c^4 : &\quad 0.51 \pm 0.07(\,(\mathrm{stat})) \pm 0.03(\,(\mathrm{syst})) \\ q^2 > 7\,\mathrm{GeV}^2/c^4 : &\quad 0.35 \pm 0.08(\,(\mathrm{stat})) \pm 0.02(\,(\mathrm{syst})) \\ q^2 \text{ integrated} : &\quad 0.43 \pm 0.06(\,(\mathrm{stat})) \pm 0.03(\,(\mathrm{syst})) \end{aligned}$$

**Table 7:** Summary of the systematic uncertainties related to the $D^*$ polarization measurement.

| Source | low $q^2$ | high $q^2$ | integrated |
|---|---|---|---|
| *Fit validation* | 0.003 | 0.002 | 0.003 |
| *FF model* | 0.007 | 0.003 | 0.005 |
| *FF parameters* | 0.013 | 0.006 | 0.011 |
| *Limited template statistics* | 0.027 | 0.017 | 0.019 |
| *Fraction of signal* $\tau^+ \to \pi^+\pi^-\pi^+\pi^0\nu_\tau$ *decays* | 0.001 | 0.001 | 0.001 |
| *Fraction of* $D^{**}$ *feed-down* | 0.001 | 0.004 | 0.003 |
| *Signal selection* | 0.005 | 0.004 | 0.005 |
| *Bin migration* | 0.008 | 0.006 | 0.007 |
| $F_L^{D^*}$ *in simulation* | 0.007 | 0.003 | 0.007 |
| $D_s^+$ *decay model* | 0.008 | 0.009 | 0.009 |
| *Shape of* $\cos\theta_D$ *template in* $D^{*-}D_s^+$ *decays* | 0.002 | 0.001 | 0.002 |
| *Shape of* $\cos\theta_D$ *template in* $D^{*-}D_s^{*+}$ *decays* | 0.007 | 0.002 | 0.004 |
| *Shape of* $\cos\theta_D$ *template in* $D^{*-}D_s^+X$ *decays* | 0.007 | 0.006 | 0.007 |
| *Shape of* $\cos\theta_D$ *template in* $D^{*-}D^+X$ *decays* | 0.002 | 0.002 | 0.003 |
| *Shape of* $\cos\theta_D$ *template in* $D^{*-}D^0X$ *decays* | 0.002 | 0.002 | 0.003 |
| $F_L^{D^*}$ *integration method* | - | - | 0.002 |
| Total | 0.036 | 0.023 | 0.029 |

## 6. Prospects

Further LFU violation tests are planned in the LHCb experiment, extending both the precision and the scope of the measurements. The results based on the full Run1+ Run2 LHC data, taken between 2011 and 2018 will be released in one or two years from now for R(Dstarm) and R($D$). LFU tests based on other $B$ hadrons, namely $B_s^0$, $B_c^+$ or $\Lambda_b^0$ hadrons should also be available in a similar time scale. The precision of these measurements has been estimated in Ref. [7] and should range between 15% and 3% depending on the hadron species (Fig. 11).

In addition, a full angular analysis of the $B^0 \to D^{*-}\tau^+\nu_\tau$ should allow to measure the complete set of the 12 coefficients governing this decay as explained in [49]. We are therefore hopeful that, at the end of the decade or maybe even sooner, taking into account the soon-to-come Belle-II results on some of these channels, a clear answer of the existence or not of LFU violation in semitauonic $B$ decays will be available!

## 7. Conclusion

Three complementary tests of Lepton Flavour Universality (LFU) using semitauonic $B$ decays performed by the LHCb collaboration are reported : the first LHCb combined measurement of R($D^{*-}$) and R($D^0$) using muonic $\tau$ decay channel, the update of the R($D^{*-}$) measurement based on hadronic $\tau$ decay channel and the first LHCb measurement of the $D^{*-}$ polarization in this decay channel. The two latter measurements are the most precise signle measurements to date. In particular, using 2 fb$^{-1}$ of proton-proton collision data at a centre-of-

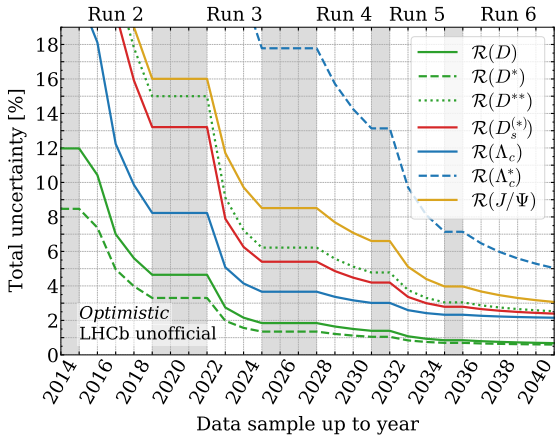


**Figure 11:** Projections of the expected precision on the various LFU R ratios as function of time, using optimistic assumptions regarding the data taking and analysis rate, and the level of the systematic floor. When confronted to real life, these curves may move to the right (slower data taking) and/or upwards (larger systematic uncertainties).

mass energy of 13 TeV, the ratio $\mathcal{B}(B^0 \to D^{*-}\tau^+\nu_\tau)/\mathcal{B}(B^0 \to D^{*-}\pi^+\pi^-\pi^+)$ is found be $1.70 \pm 0.10^{+0.11}_{-0.10}$, where the first uncertainty is statistical and the second systematic. The lepton universality test, $\mathcal{R}(D^{*-}) \equiv \mathcal{B}(B^0 \to D^{*-}\tau^+\nu_\tau)/\mathcal{B}(B^0 \to D^{*-}\mu^+\nu_\mu)$ is found to be $0.257 \pm 0.012\,(\text{stat}) \pm 0.014\,(\text{syst}) \pm 0.012$ (ext), after inclusion of the previously published Run1 result. This result is compatible with SM prediction and with previous measurements. Using these recent LHCb results, the updated word average R($D^*$) and R($D$) however still displays a 3.3 $\sigma$ disagreement with the SM prediction.

The $D^{*-}$ polarization, which is a powerful complementary test of a potential LFU violation, has been measured for the first by the LHCb collaboration using the same hadronic semitauonic $B^0$ decays in two $q^2$ bins and been found to be: $0.51 \pm 0.07\,(\text{stat}) \pm 0.03\,(\text{syst})$, $0.35 \pm 0.08\,(\text{stat}) \pm 0.02\,(\text{syst})$ and $0.43 \pm 0.06\,(\text{stat}) \pm 0.03\,(\text{syst})$, for $q^2$ below 7 GeV$^2/c^4$, above 7 GeV$^2/c^4$ and integrated over all $q^2$ values, respectively. This result, the most precise to date, is compatible with SM predictions and could potentially exclude some phase space regions of New Physics models where the polarization is very different from SM expectations. In the coming years, the expected new results from LHCb and Belle-II collaborations should allow to answer in a clear way to the existence or not of LFU violations in semitauonic $B$ decays.

## References

[1] BaBar collaboration, J. P. Lees *et al.*, *Evidence for an excess of $\bar{B} \to D^{(*)}\tau^-\bar{\nu}_\tau$ decays*, Phys. Rev. Lett. **109** (2012) 101802, arXiv:1205.5442.

[2] Belle collaboration, M. Huschle *et al.*, *Measurement of the branching ratio of $\bar{B} \to D^{(*)}\tau^-\bar{\nu}_\tau$ relative to $\bar{B} \to D^{(*)}\ell^-\bar{\nu}_\ell$ decays with hadronic tagging at Belle*, Phys. Rev. **D92** (2015) 072014, arXiv:1507.03233.

[3] Belle collaboration, S. Hirose *et al.*, *Measurement of the $\tau$ lepton polarization and $R(D^*)$ in the decay $\bar{B} \to D^*\tau^-\bar{\nu}_\tau$ with one-prong hadronic $\tau$ decays at Belle*, Phys. Rev. **D97** (2018) 012004, arXiv:1709.00129.

[4] LHCb collaboration, R. Aaij *et al.*, *Measurement of the ratio of branching fractions $\mathcal{B}(\bar{B}^0 \to D^{*+}\tau^-\bar{\nu}_\tau)/\mathcal{B}(\bar{B}^0 \to D^{*+}\mu^-\bar{\nu}_\mu)$*, Phys. Rev. Lett. **115** (2015) 111803, Publisher's Note ibid. **115** (2015) 159901, arXiv:1506.08614.

[5] LHCb collaboration, R. Aaij *et al.*, *Measurement of the ratio of the $\mathcal{B}(B^0 \to D^{*-}\tau^+\nu_\tau)$ and $\mathcal{B}(B^0 \to D^{*-}\mu^+\nu_\mu)$ branching fractions using three-prong $\tau$-lepton decays*, Phys. Rev. Lett. **120** (2018) 171802, arXiv:1708.08856.

[6] LHCb collaboration, R. Aaij *et al.*, *Test of lepton flavor universality by the measurement of the $B^0 \to D^{*-}\tau^+\nu_\tau$ branching fraction using three-prong $\tau$ decays*, Phys. Rev. **D97** (2018) 072013, arXiv:1711.02505.

[7] F. U. Bernlochner, M. Franco Sevilla, D. J. Robinson, and G. Wormser, *Semitauonic b-hadron decays: A lepton flavor universality laboratory*, Rev. Mod. Phys. **94** (2022) 015003.

[8] Y. Amhis *et al.*, *Averages of b-hadron, c-hadron, and $\tau$-lepton properties as of 2021*, Phys. Rev. D **107** (2023) 052008, arXiv:2206.07501, The updated plots regarding LFU tests are located on this web page https://hflav.web.cern.ch/content/semileptonic-b-decays.

[9] Belle-2 collaboration, K. Kojima, *Recent Belle II results on semileptonic ! decays and tests of lepton-flavor universality*, 2023. Talk presented at the 31st international Lepton-Photon conference , Hamburg, August 2023.

[10] S. Fajfer, J. F. Kamenik, and I. Nisandzic, *On the $B \to D^*\tau\bar{\nu}_\tau$ sensitivity to new physics*, Phys. Rev. **D85** (2012) 094025, arXiv:1203.2654.

[11] S. Fajfer and N. Košnik, *Vector leptoquark resolution of $R_K$ and $R_{D^{(*)}}$ puzzles*, Physics Letters B **755** (2016) 270–274, arXiv:1511.06024.

[12] A. Crivellin, D. Müller, and T. Ota, *Simultaneous explanation of $R(D^{(*)})$ and $b \to s\mu^+\mu^-$: the last scalar leptoquarks standing*, JHEP **2017** (2017) 40, arXiv:1703.09226.

[13] A. K. Alok, D. Kumar, S. Kumbhakar, and S. U. Sankar, *$D^*$ polarization as a probe to discriminate new physics in $\overline{B} \to D^*\tau\overline{\nu}$*, Phys. Rev. D **95** (2017) 115038, arXiv:1606.03164.

[14] M. A. Ivanov, J. G. Körner, and C. T. Tran, *Analyzing new physics in the decays $\overline{B}^0 \to D^{(*)}\tau^-\overline{\nu}_\tau$ with form factors obtained from the covariant quark model*, Phys. Rev. D **94** (2016) 094028, arXiv:1607.02932.

[15] LHCb collaboration, A. A. Alves Jr. *et al.*, *The LHCb detector at the LHC*, JINST **3** (2008) S08005.

[16] LHCb collaboration, R. Aaij *et al.*, *LHCb detector performance*, Int. J. Mod. Phys. **A30** (2015) 1530022, arXiv:1412.6352.

[17] R. Aaij *et al.*, *Performance of the LHCb Vertex Locator*, JINST **9** (2014) P09007, arXiv:1405.7808.

[18] R. Arink *et al.*, *Performance of the LHCb Outer Tracker*, JINST **9** (2014) P01002, arXiv:1311.3893.

[19] P. d'Argent *et al.*, *Improved performance of the LHCb Outer Tracker in LHC Run 2*, JINST **12** (2017) P11016, arXiv:1708.00819.

[20] M. Adinolfi *et al.*, *Performance of the LHCb RICH detector at the LHC*, Eur. Phys. J. **C73** (2013) 2431, arXiv:1211.6759.

[21] A. A. Alves Jr. *et al.*, *Performance of the LHCb muon system*, JINST **8** (2013) P02022, arXiv:1211.1346.

[22] R. Aaij *et al.*, *The LHCb trigger and its performance in 2011*, JINST **8** (2013) P04022, arXiv:1211.3055.

[23] V. V. Gligorov and M. Williams, *Efficient, reliable and fast high-level triggering using a bonsai boosted decision tree*, JINST **8** (2013) P02013, arXiv:1210.6861.

[24] T. Likhomanenko *et al.*, *LHCb topological trigger reoptimization*, J. Phys. Conf. Ser. **664** (2015) 082025, arXiv:1510.00572.

[25] D. Müller, M. Clemencic, G. Corti, and M. Gersabeck, *ReDecay: A novel approach to speed up the simulation at LHCb*, Eur. Phys. J. **C78** (2018) 1009, arXiv:1810.10362.

[26] LHCb collaboration, R. Aaij *et al.*, *Measurement of the ratio of branching fractions $\mathcal{R}(D^*)$ and $\mathcal{R}(D^0)$* , Phys. Rev. Lett. **131** (2023) 111802, arXiv:2302.02886.

[27] LHCb collaboration, R. Aaij *et al.*, *Test of lepton flavour universality using $B^0 \to D^{*-}\tau^+\nu_\tau$ decays, with hadronic $\tau$ channels*, Phys. Rev. **D108** (2023) 012018, arXiv:2305.01463.

[28] LHCb collaboration, R. Aaij *et al.*, *A precise measurement of the $B^0$ meson oscillation frequency*, Eur. Phys. J. **C76** (2016) 412, arXiv:1604.03475.

[29] Particle Data Group, R. L. Workman *et al.*, *Review of particle physics*, Prog. Theor. Exp. Phys. **2022** (2022) 083C01.

[30] BES-III collaboration, M. Ablikim *et al.*, *Measurement of the absolute branching fraction of the inclusive decay $D_s^+ \to \pi^+\pi^-\pi^+X$*, Physical Review D **108** (2023) .

[31] T. Skwarnicki, *A study of the radiative cascade transitions between the Upsilon-prime and Upsilon resonances*, PhD thesis, Institute of Nuclear Physics, Krakow, 1986, DESY-F31-86-02.

[32] LHCb collaboration, R. Aaij *et al.*, *TBD*, LHCb-PAPER-2023-020, in preparation.

[33] S. Fajfer, J. F. Kamenik, and I. Nišandžić, *On the $B \to D^*\tau\bar{\nu}_\tau$ sensitivity to new physics*, Phys. Rev. D **85** (2012) 094025, arXiv:1203.2654.

[34] M. A. Ivanov, J. G. Körner, and C. T. Tran, *Analyzing new physics in the decays $\overline{B}^0 \to D^{(*)}\tau^-\overline{\nu}_\tau$ with form factors obtained from the covariant quark model*, Phys. Rev. D **94** (2016) 094028, arXiv:1607.02932.

[35] Belle collaboration, A. Abdesselam *et al.*, *Measurement of the $D^{*-}$ polarization in the decay $B^0 \to D^{*-}\tau^+\nu_\tau$*, in *10th International Workshop on the CKM Unitarity Triangle*, 2019, arXiv:1903.03102.

[36] M. A. Ivanov, J. G. Körner, and C. T. Tran, *Exclusive decays $B \to \ell^-\overline{\nu}$ and $B \to D^{(*)}\ell^-\overline{\nu}$ in the covariant quark model*, Phys. Rev. D **92** (2015) 114022, arXiv:1508.02678.

[37] M. Tanaka and R. Watanabe, *New physics in the weak interaction of $\overline{B} \to D^{(*)}\tau\overline{\nu}$*, Phys. Rev. D **87** (2013) 034028, arXiv:1212.1878.

[38] A. K. Alok, D. Kumar, S. Kumbhakar, and S. U. Sankar, *$D^*$ polarization as a probe to discriminate new physics in $\overline{B} \to D^*\tau\overline{\nu}$*, Phys. Rev. D **95** (2017) 115038, arXiv:1606.03164.

[39] Z.-R. Huang *et al.*, *Footprints of new physics in $b \to c\tau\nu$ transitions*, Phys. Rev. D **98** (2018) 095018, arXiv:1808.03565.

[40] S. Bhattacharya, S. Nandi, and S. K. Patra, *$b \to c\tau\nu$ decays: a catalogue to compare, constrain, and correlate new physics effects*, The European Physical Journal C **79** (2019) , arXiv:1805.08222.

[41] M. Bordone, N. Gubernari, D. van Dyk, and M. Jung, *Heavy-quark expansion for $\bar{B}_s \to D_s^{(*)}$ form factors and unitarity bounds beyond the $SU(3)_F$ limit*, The European Physical Journal C **80** (2020) , arXiv:1912.09335.

[42] D. Bečirević, M. Fedele, I. Nišandžić, and A. Tayduganov, *Lepton flavor universality tests through angular observables of $\overline{B} \to D^{(*)}\ell\overline{\nu}$ decay modes*, arXiv:1907.02257.

[43] I. Caprini, L. Lellouch, and M. Neubert, *Dispersive bounds on the shape of form factors*, Nuclear Physics B **530** (1998) 153–181, arXiv:hep-ph/9712417.

[44] F. U. Bernlochner *et al.*, *Das ist der HAMMER: Consistent new physics interpretations of semileptonic decays*, Eur. Phys. J. C **80** (2020) 883, arXiv:2002.00020.

[45] J. G. Pardiñas *et al.*, *RooHammerModel: interfacing the HAMMER software tool with HistFactory and RooFit*, Journal of Instrumentation **17** (2022) T04006, arXiv:2007.12605.

[46] M. Pivk and F. R. Le Diberder, *sPlot: A statistical tool to unfold data distributions*, Nucl. Instrum. Meth. **A555** (2005) 356, arXiv:physics/0402083.

[47] C. G. Boyd, B. Grinstein, and R. F. Lebed, *Precision corrections to dispersive bounds on form factors*, doi: 10.1103/physrevd.56.6895 arXiv:hep-ph/9705252.

[48] F. U. Bernlochner, Z. Ligeti, M. Papucci, and D. J. Robinson, *Combined analysis of semileptonic b decays to d and d*: R(d(*)), |vcb|, and new physics*, Physical Review D **95** (2017) .

[49] D. Hill, M. John, W. Ke, and A. Poluektov, *Model-independent method for measuring the angular coefficients of b0 → d*τν_τdecays*, Journal of High Energy Physics **2019** (2019) .